AGU PUBLICATIONS

JGR

Journal of Geophysical Research: Space Physics

BRIEF REPORT

10.1002/2014JA020113

Key Points:
- Address valley region irregularities at and off equator
- Use capacitor analogy of plasma bubble for estimating fringe field
- Show how fringe field diminishes with latitude resulting in no irregularities

Correspondence to:
A. K. Patra,
akpatra@narl.gov.in

Citation:
Mukherjee, S., and A. K. Patra (2014), Parallel plate capacitor analogy of equatorial plasma bubble and associated fringe fields with implications to equatorial valley region irregularities, *J. Geophys. Res. Space Physics*, *119*, 6631–6641, doi:10.1002/2014JA020113.

Received 24 APR 2014
Accepted 3 AUG 2014
Accepted article online 6 AUG 2014
Published online 22 AUG 2014

Parallel plate capacitor analogy of equatorial plasma bubble and associated fringe fields with implications to equatorial valley region irregularities

S. Mukherjee[1] and A. K. Patra[2]

[1]Department of Physics, Indian Institute of Technology, Kharagpur, India, [2]National Atmospheric Research Laboratory, Gadanki, India

Abstract VHF radar echoes from the valley region plasma irregularities, displaying ascending pattern, are often observed during the active phase of equatorial plasma bubble in the close vicinity of the geomagnetic equator and have been attributed to bubble-related fringe field effect. These irregularities however are not observed at a few degrees away from the equator. In this paper, we attempt to understand this contrasting observational result by comparing fringe field at the geomagnetic equator and low latitudes. We use parallel plate capacitor analogy of equatorial plasma bubble and choose a few capacitor configurations, consistent with commonly observed dimension and magnetic field-aligned property of plasma bubble, for computing fringe field. Results show that fringe field decreases significantly with decreasing altitude as expected. Further, fringe field decreases remarkably with latitude, which clearly indicates the role of magnetic field-aligned property of plasma bubble in reducing the magnitude of fringe field at low latitudes compared to that at the geomagnetic equator. The results are presented and discussed in the light of current understanding of plasma bubble-associated fringe field-induced plasma irregularities in the valley region.

1. Introduction

Radar echoes from the valley region, displaying ascending echoing pattern, in association with *F* region plume structures in the Jicamarca radar observations [e.g., *Woodman and LaHoz*, 1976; *Hysell et al.*, 1990; *Woodman and Chau*, 2001], continue to be elusive in terms of their origin. For illustration, an example of Jicamarca observation, presented earlier by *Woodman and Chau* [2001], is reproduced in Figure 1. Note the ascending pattern of the valley region echoes, which extends gradually to altitudes as high as 300 km. Doppler velocities (not shown here) of these echoes were upward, representing eastward electric field. Valley region echoes of similar kind were also reported from São Luis, a Brazilian equatorial location [*Alam Kherani et al.*, 2012]. These observations imply the presence of small-scale plasma irregularities with scale sizes (3–5 m) that match the Bragg scattering condition ($\lambda_{\text{irregularity}} = \lambda_{\text{radar}}/2$) in the valley region. These meter-scale irregularities are believed to be generated through a turbulence cascade from irregularities at larger scale than a few meters. *Woodman* [1993] suggested that these valley region irregularities could be generated while *E* region plasma is uplifted by the fringe electric fields associated with the growth phase of the equatorial plasma bubble [*Zalesak and Ossakow*, 1980]. Although this interpretation was quite consistent with the fact that plasma inside the depleted regions has extremely low density and comprises metallic ions [*Hanson and Sanatani*, 1971; *Hanson et al.*, 1972], which are formed in the *E* region by meteoric ablation process, no analysis on the fringe field and their effect was made at that time. Later, *Alam Kherani et al.* [2002, 2004], using numerical simulation, attempted to study the effect of fringe fields associated with the generalized Rayleigh–Taylor instability on the valley and *E* regions in order to explain the valley region irregularities. *Alam Kherani et al.* [2004] however found that the fringe fields could not penetrate into the *E* region due to increasing collision with decreasing altitude but could reasonably penetrate to the upper *E* region (120 km). They suggested that the *E* region irregularities occurring close to 120 km can be effectively pulled up by the fringe field to the valley region and above explaining their occurrence in the valley region.

Valley region echoing structures of the type observed at Jicamarca and São Luis in association with overhead *F* region irregularities [e.g., *Woodman and Chau*, 2001; *Alam Kherani et al.*, 2012] however have not been

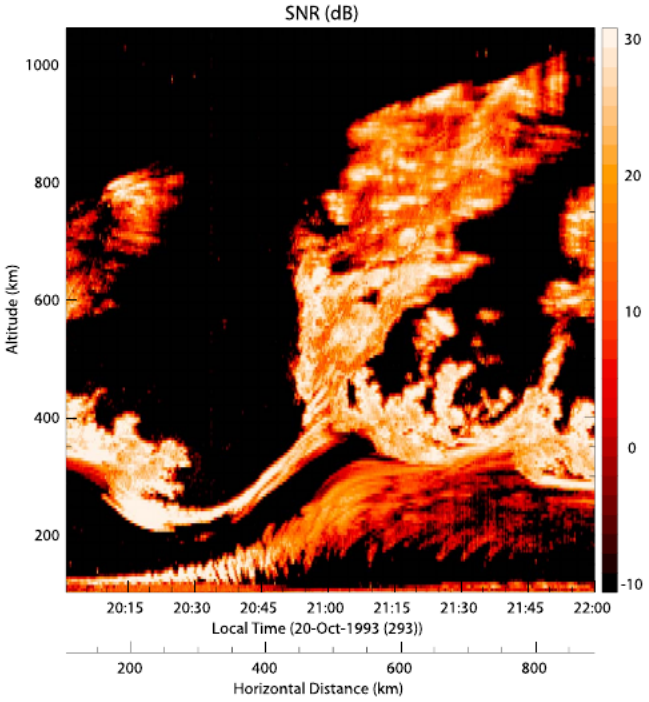

Figure 1. Height-time-SNR map of ionospheric irregularities observed in the *E* and *F* regions by the Jicamarca radar [reproduced from *Woodman and Chau*, 2001]. Note the ascending echoing structures in the valley region during the updraft of the *F* region irregularities and plume structures.

observed at Gadanki, located at 6.5°N magnetic latitude [*Patra and Rao*, 2007]. *Patra and Rao* [2007] however found that valley region irregularities do occur over Gadanki, but at a later time (typically after 21 LT). Notably, these irregularities occur even if *F* region irregularities do not exist overhead. Moreover, in the height time intensity map, the valley region irregularities over Gadanki are found to display descending pattern reminiscent of intermediate layer [*Patra et al.*, 2002; *Patra and Rao*, 2007]. It is also important to mention that while some of these irregularities at times show ascending structures (Figure 2d of *Patra and Rao* [2007]) having some resemblance to those of Jicamarca observations reported by *Woodman and Chau* [2001], they are not associated with overhead *F* region irregularities and are also very limited in number. They are more close to the so-called quasiperiodic echoes [*Yamamoto et al.*, 1991] extending to higher altitudes than those commonly observed as quasiperiodic echoes at Gadanki [*Choudhary et al.*, 2005; *Venkateswara Rao et al.*, 2008]. Importantly, Doppler velocities of the valley region echoes over Gadanki reported by *Patra and Rao* [2007] are predominantly downward (their Figures 5 and 6), which is in sharp contrast to those observed as upward velocities by *Woodman and Chau* [2001]. Valley region irregularities, displaying descending pattern similar to those of Gadanki, have also been reported from Kototabang, located at 10.6°S magnetic latitude in Indonesia [*Yokoyama et al.*, 2005]. Further, no ascending structures of valley region irregularities have been observed over Kototabang during the growth phase of overhead *F* region irregularities consistent with those observed over Gadanki. Importantly, both at Gadanki and Kototabang, valley region

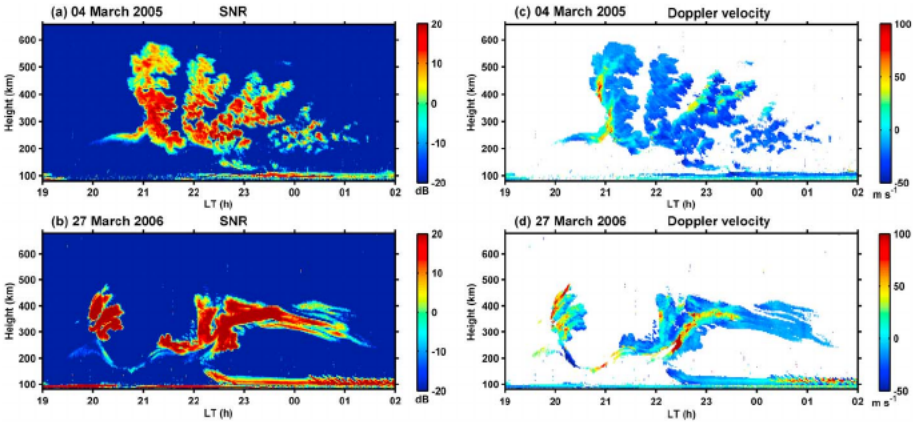

Figure 2. Height-time-SNR map of ionospheric irregularities observed by the Gadanki radar on (a) 4 March 2005 and (b) 27 March 2006. Height-time velocity maps are shown in (c) 4 March 2005 and (d) 27 March 2006. Note that there are no valley region irregularities during the updraft of the *F* region irregularities, and plume structures and valley region irregularities observed at a later stage show descending pattern with downward Doppler velocity.

irregularities are not observed during the growth phase of plasma bubble, and hence, they are strikingly different from those of Jicamarca.

To demonstrate these features, two examples of Gadanki radar observations made on 4 March 2005 and 27 March 2006, displaying the occurrence of *E* and *F* region irregularities, are shown in Figures 2a and 2b, respectively. Note the clear bottomside band structure displaying a sinusoidal pattern observed on 27 March 2006. On 4 March 2005, while the first plume occurred around 21 LT, on 27 March 2006, the first plume occurred around 20 LT. For the early plume activities, the time intervals between two successive plumes varied between 1 and 2 h. Assuming frozen in condition of the structures and zonal plasma drift of 100 m s^{-1} (which is very typical in the evening hours), interplume time separation of 1–2 h implies a horizontal separation of 360–720 km. These separations are very similar to those shown by *Woodman and Chau* [2001]. There are also closely separated plumes with time scales of 20–30 min, which would imply a horizontal separation of 120–180 km. On the other hand, the duration of plume varies from 20 min to 1 h, which implies east-west plume dimensions of 90–360 km. Importantly, note that in both the examples, no valley region echoes were observed in the postsunset hours, while the fully blown *F* region plume structures were observed. The valley region irregularities however were observed at a later time (after 22:15 LT) when the overhead *F* region irregularities are in their decay phase consistent with observations reported earlier by *Patra and Rao* [2007]. Note that the echoes from the valley region irregularities were stronger on 27 March 2006 than on 4 March 2005. Signal-to-noise ratio (SNR) values were as large as 20 dB and 40 dB above noise on 4 March and 27 March, respectively. Radar echoes from valley region irregularities reported by *Woodman and Chau* [2001] were also found to have similar SNR except the fact that they were observed during 20–22 LT. It is important to mention that not observing the valley region irregularities during the postsunset hours is not linked with the sensitivity of the Gadanki radar, since this radar is capable of detecting much weaker echoes such as those associated with daytime 150 km echoing phenomenon occurring in the same height region [*Patra and Rao*, 2006]. Moreover, since the sensitivity of the Gadanki radar is only 3 dB lower than that of Jicamarca for *F* region irregularity observations (which use transmitter power of $\leq$1 MW) and the SNR dynamic range of the valley region echoes observed by the Jicamarca radar is 40 dB, it is very unlikely that the Gadanki radar would miss these if they are present. Drift velocities of the irregularities observed on 4 March 2005 and 27 March 2006 are presented in Figures 2c and 2d, respectively. Positive (negative) velocity represents upward (downward) irregularity drift. Note the downward drifts of the valley region irregularities in both examples, which are opposite to those observed as upward drifts by *Woodman and Chau* [2001]. The phenomenology of the nighttime irregularities observed over Gadanki described above is very common and is different from that observed over Jicamarca [*Woodman and Chau*, 2001].

Given the fact that plasma bubble grows as flux tube-integrated entity; i.e., it grows vertically and along the magnetic field simultaneously, not observing these irregularities at off-equatorial location raises an important question on the validity of the interpretation of the equatorial ascending type valley region irregularities in terms of plasma bubble-related fringe field. Here it may be mentioned that it has not yet been clear whether the fringe fields are responsible for the generation of the valley region irregularities or they transport the already existing *E* region irregularities upward into the valley region. Given the fact that ascending type valley region irregularity structures are not observed on every plasma bubble event at Jicamarca, it is quite possible that fringe field transport the upper *E* region irregularities into the valley region. On the other hand, since ascending type valley region irregularities are not observed even when *E* region irregularities are observed at low latitudes such as Gadanki and Kototabang, it would be relevant to examine whether bubble-associated fringe field changes with latitude. Fringe field computations [*Alam Kherani et al.*, 2002, 2004] however have been performed for the equatorial magnetic field geometry, and it is not known how the fringe fields would vary from horizontal to inclined magnetic field geometry.

In this work, we use a parallel plate capacitor analogy of the equatorial plasma bubble and estimate fringe fields as a function of decreasing height, following analytical expressions given by *Parker* [2002]. The shapes of the capacitor plates are chosen in such a manner that the penetration of fringe fields can be defined for both horizontal and inclined magnetic field geometries for making a comparison between the two. Results show noticeable reduction in the fringe field as a function of latitude and decreasing altitude. These results are presented and discussed in the light of current understanding of the fringe field effects in the ionospheric plasma transport and formation/upward transport of irregularities.

2. Fringe Field in Parallel Plate Capacitor

When a parallel plate capacitor with a plate area of A and an interplate separation distance d is filled with a dielectric of permittivity ε and subjected to a potential V, the capacitance C and electric field E between the plates can be calculated as

$$C = Q/V, \tag{1}$$

$$E = V/d = Q/\varepsilon A, \tag{2}$$

where Q is the total charge accumulated on the plate. Measured capacitance and electric field however differ from theoretical value. These effects are explained in terms of fringe field effects.

Parker [2002] provided a theoretical framework and obtained analytic expressions for electric field outside a strip capacitor. He used a parallel plate capacitor composed of two plates, each having length L and width W ($W \ll L$) and plate separation of d ($d \ll L$ and W), which are assigned with potentials of $\pm V/2$. *Parker* [2002] expressed potential V as a function of interplate distance d as

$$V = Kd, \tag{3}$$

where K is a constant, which depends on the magnitude of the charge per unit area on the inside surfaces of the plate. *Parker* [2002] simplified the above-mentioned configuration in such a way that the configuration becomes two dimensional; i.e., the cross section of the parallel plates is in the $x = 0$ plane, d parallel to z axis, and L parallel to y axis. Then by using the symmetry about zero potential, which is along the z axis, *Parker* [2002] obtained two components of electric field as

$$E_z(y,z) = \left(\frac{V}{2\pi}\right)\left[\frac{\frac{W}{2}+y}{\left[z^2+\left(\frac{W}{2}+y\right)^2\right]}+\frac{\frac{W}{2}-y}{\left[z^2+\left(\frac{W}{2}-y\right)^2\right]}\right], \tag{4}$$

$$E_y(y,z) = \left(\frac{-Vz}{2\pi}\right)\left[\frac{1}{\left[z^2+\left(\frac{W}{2}+y\right)^2\right]}-\frac{1}{\left[z^2+\left(\frac{W}{2}-y\right)^2\right]}\right], \tag{5}$$

where E_z and E_y are the electric field components along d and L, respectively. The fields become infinite at the end because infinitely thin plates are assumed. Electric field lines outside the plate in the y-z plane are given as

$$\frac{dz}{dy} = \frac{E_z}{E_y} = \frac{z^2 - y^2 + \frac{W^2}{4}}{2yz} \tag{6}$$

Then by shifting the origin along y axis by $W/2$, i.e., $z' = z, \quad y' = y - \frac{W}{2}$, equation (6) for arbitrary value of W is rewritten as

$$\frac{dz'}{dy'} = \frac{E_z}{E_y} = \frac{z'^2 - y'^2 - y'W}{2y'z' + z'W}. \tag{7}$$

The solution of equation (7), for $z' > 0$ is given as [*Parker*, 2002]

$$z'(y') = \left(\frac{1}{2}\right)\sqrt{W+2y'}\sqrt{C - \frac{W^2 + 2Wy' + 4y'^2}{W+2y'}}. \tag{8}$$

In the case of $C > W$, the allowed range of y' for lines in the right half of the y-z plane, i.e., $y'_- < y' < y'_+$, is given as

$$y'_{\mp} = \frac{C-W}{4}\left[1 \mp \sqrt{1 + \frac{4W}{C-W}}\right]. \tag{9}$$

More details on the formulation and mathematical treatment used in deriving fringe fields can be found in *Parker* [2002].

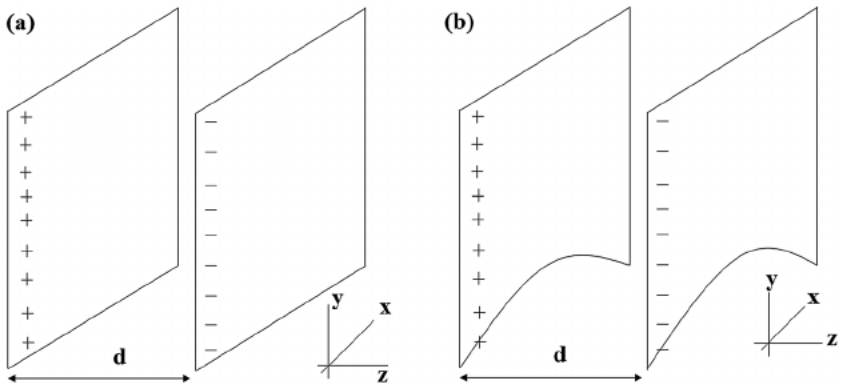

Figure 3. Parallel plate capacitors with (a) flat edge at the bottom and (b) curved edge at the bottom. The coordinate system is also shown. For computation, the origin of the coordinate system has been taken at the midpoint of the line joining the centers of the top flat edges of the capacitor plates.

3. Fringe Field Computation

In the present work, we have performed fringe field computation for two different configurations of parallel plate capacitor. These two configurations are shown in Figures 3a and 3b, respectively. Configuration 1 consists of two rectangular parallel plates having length (L), breadth (W), and interplate separation (d) in such a way that they are equivalent to 400 km in the vertical, 1200 km in the north-south, and 100 km in the east-west directions, respectively. Configuration 2 consists of two plates with similar dimensions as that of configuration 1 but with the bottom edge having a curvature, which is an approximation for low-latitude magnetic field geometry. The curved edge is chosen in such a way that it is elongated along north-south and symmetric about the magnetic equator. Considering the fact that plasma bubble maps along magnetic field lines and magnetic field lines at low latitudes have finite dip angle, this configuration has been chosen. Thus, while configuration 1 is applicable to the magnetic equator, where the magnetic field is horizontal, configuration 2 can be used for low latitudes, where magnetic field lines are tilted, as well as at the equator. Moreover, fringe fields of these configurations can also be used to understand the equatorial and low-latitude observations of valley region irregularities mentioned in the Introduction.

In the adopted coordinate system, described in section 2, x is parallel to north-south, y is parallel to vertical direction, and z is parallel to the interplate separation, which is parallel to east-west direction. For computation, the origin of the coordinate system however has been taken at the midpoint of the line joining the centers of the top flat edges of the capacitor plates. In the present case, we are primarily concerned with the east-west electric field, E_z, that is responsible for the up-down motion of plasma. E_z component of fringe field is computed following equation (4) as a function of decreasing altitude, which is parallel to y axis and in the vertical downward direction. The coordinates through which the field lines would pass are obtained from equations (8) and (9). For our convenience in numerical computation and for obtaining the required shape of the fringes, we have chosen the integration constant C in equations (8) and (9) in the increasing order of field lines as it goes away from the plate. They are as follows:

$$C = 1.02, 1.10, 1.25, 1.50, 2\,(\text{for 100 km plate separation})$$

$$C = 0.45, 0.60, 0.65, 0.73, 0.88\,(\text{for 200 km plate separation}).$$

Equations (4–9) however are applicable for a strip capacitor, and here we need to obtain the fringe fields for configuration 1 and configuration 2, which have finite W (in the present case 1200 km). One possible way is to integrate the fringe fields of several such strip capacitors. In the present study, for simplicity, we have used seven plate capacitors in such a way that they form the shape shown in configuration 1. Each of these plate capacitors consists of 60 strip capacitors. Then the fringe fields of these strip capacitors are integrated, and the east-west components of electric fields (i.e., E_z) outside the plate capacitor in the y-z plane (i.e., east-west component of fringe field) are used for our consideration. For the second configuration, seven small plate capacitors have been used to obtain an equivalent plate capacitor. These plates are oriented in such a manner that they approximately form the shape of the configuration 2. Then the resultant fringe fields in the east-west plane are computed.

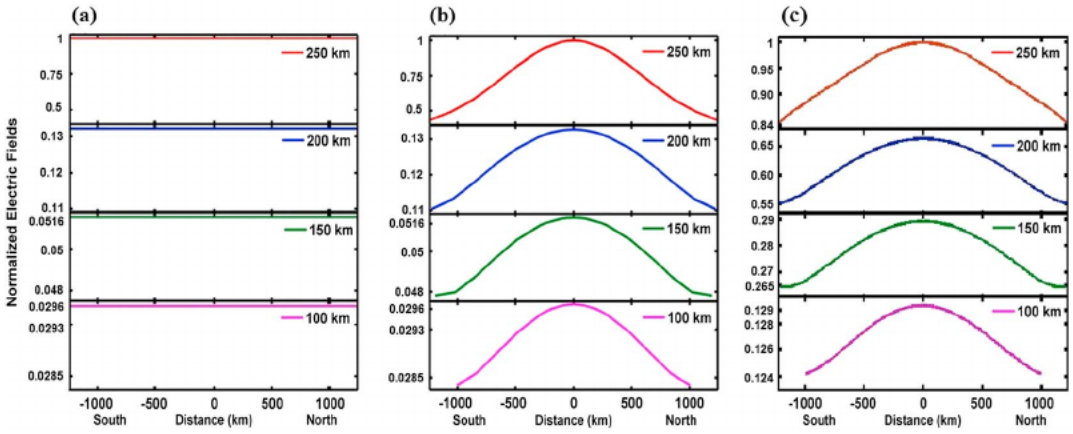

Figure 4. Distributions of normalized fringe electric field as a function of height and latitude along the north-south for (a) configuration 1 with $L = 400$ km, $W = 1200$ km, and $d = 100$ km; (b) configuration 2 with $L = 400$ km, $W = 1200$ km, and $d = 100$ km; and (c) configuration 2 with $L = 400$ km, $W = 1200$ km, and $d = 200$ km. In these figures, electric field is directed eastward.

The capacitors shown in Figure 3 are assumed to be located at an altitude of 300 km so that fringe fields below this altitude can be computed for their application to the ionospheric phenomenon chosen in this work. Given the fact that the base of plasma bubble lies around 300 km, the above assumption is quite realistic.

4. Results and Discussion

First, we address how fringe field varies along north-south for configuration 1 and configuration 2. It may be mentioned that fringe fields are directed eastward. Figures 4a and 4b show peak values of fringe field, which maximize at midpoints of the capacitors, for configuration 1 and configuration 2, respectively. Fringe fields have been computed for $L = 400$ km, $W = 1200$ km, and $d = 100$ km. All fringe fields have been normalized to unity and plotted in different scales for different heights for clarity. In the case of configuration 1, fringe field decreases with altitude but does not change along north-south. In contrast to this, fringe field in configuration 2 not only decreases with height, it decreases remarkably along north-south. Fringe field attains a maximum value at the center, i.e., at the equator, and the percentage decrease in the normalized electric field over the equator at altitudes of 200 km, 150 km, and 100 km with respect to that at 250 km are 86.73%, 94.83%, and 97.03%, respectively. In the case of configuration 2, fringe field is found to decrease along north-south also. For example, corresponding to the 250 km altitude, the fringe field at a distance of 1200 km from the equator becomes 37% of that at the equator. At a similar distance from the equator, fringe field reduces remarkably at lower altitudes, and at an altitude of 100 km, the fringe field becomes negligibly small.

Figure 4c shows results for configuration 2 having $L = 400$ km, $W = 1200$ km, and $d = 200$ km. Interestingly, in this case, fringe field does not decrease as fast as that of configuration 2 having $d = 100$ km both vertically and along north-south, implying that fringe field can easily penetrate downward and extend along north-south if the width is increased. Note that the normalized electric fields are higher than those for $d = 100$ km. For example, at 250 km altitude, the fringe field at a distance of 1200 km from the equator becomes about 85% of that at the equator. This arises due to equation (3) that suggests that the potential V is proportional to the interplate distance d.

In order to examine fringe field for large bubble, we have considered a case with zonal dimension of 500 km consistent with some of the large bubbles shown in Figure 2. Computation has been done in the same way as has been done for $d = 100$ km and 200 km, except that in the present case, the values of C are 0.23, 0.34, 0.38, 0.42, and 0.52. Variations of normalized east-west fringe field along north-south direction at different altitudes are shown in Figure 5. Note that in this case also, fringe field decreases northward/southward from the equator as well as with decreasing altitude. The decrease in the fringe field however is relatively less than those of $d = 100$ km and 200 km. We note that the fringe field reduction at low latitude is at least 10% of that at the equator.

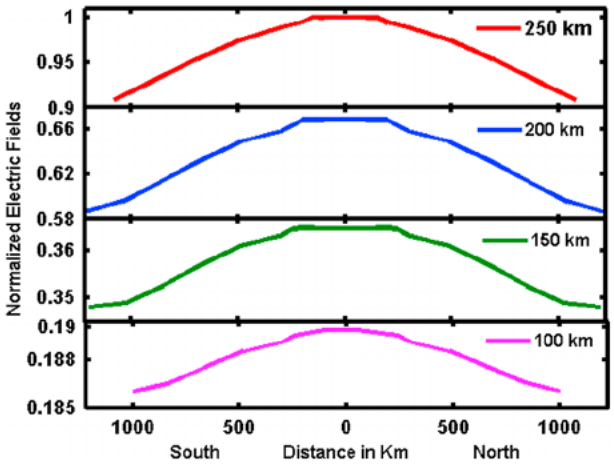

Figure 5. Same as Figure 4 but for configuration 2 with plate separation $d = 500$ km. Direction of electric field is eastward.

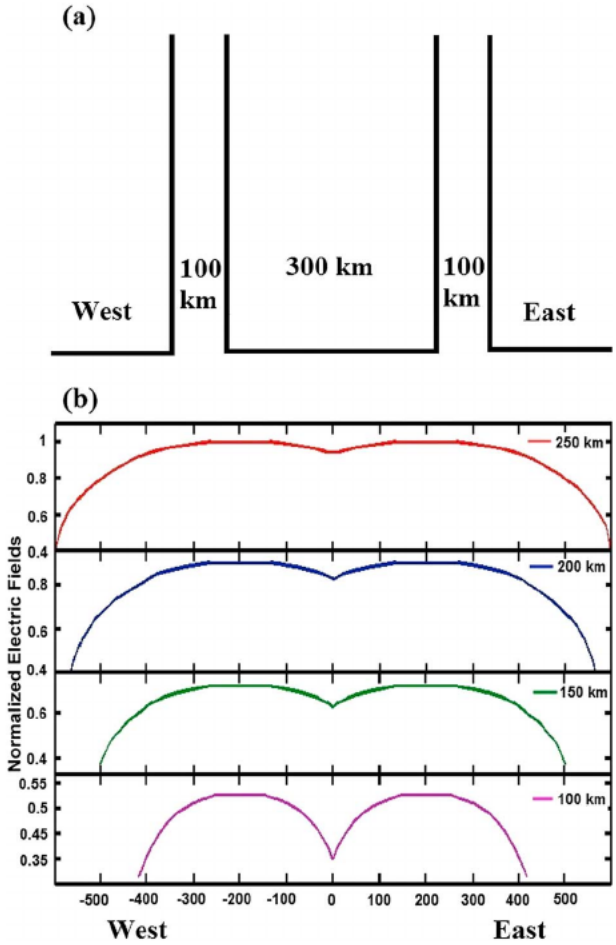

Figure 6. (a) Two parallel plate capacitors with dimensions equivalent to $L = 400$ km, $W = 1200$ km, and $d = 100$ km and separated by 300 km. (b) Distributions of normalized fringe electric field as a function of height and longitude at the magnetic equator. Direction of electric field is eastward.

Next, we present how fringe field would vary in the east-west direction when more than one plasma bubble exists. Since more than one plasma bubble can occur in the east-west direction and the zonal dimension of bubble as well as interbubble separation could vary from one day to another, we have examined variation of fringe field along east-west in such configurations. For demonstration, we have considered a pair of bubbles separated by a distance. We have chosen three cases: (1) bubbles with east-west dimension of 100 km and interbubble separation of 300 km, (2) bubbles with east-west dimension of 200 km and interbubble separation of 300 km, and (3) bubbles with east-west dimension of 500 km and interbubble separation of 500 km.

In order to perform the computation for the first case, we have considered two parallel plate capacitors having $L = 400$ km, $W = 1200$ km, and $d = 100$ km each and separated by 300 km, which is shown in Figure 6a. This configuration signifies that there are two plasma bubbles having width of 100 km each and interbubble separation of 300 km. Although in principle both width and interbubble separation could be different from those used here, this configuration is used to demonstrate how the fringe field would vary both in east-west and vertical directions. Figure 6b shows the variations in fringe field in the east-west direction and at different altitudes. As can be noted that fringe field exists everywhere in the east-west direction, be it just below the capacitor or in the region where there is no capacitor. We however note that fringe field is maximum where the central part of the capacitor is located and minimum at the farthest distance from the center of the capacitor. Again, fringe field decreases with decreasing height.

Figures 7a and 7b show results similar to that of Figure 6 but for $d = 200$ km. In this case, fringe field does not even drop in between the two capacitors. It looks as if there is one capacitor. This implies that if two bubbles are wide enough and the interbubble separation is of the order of

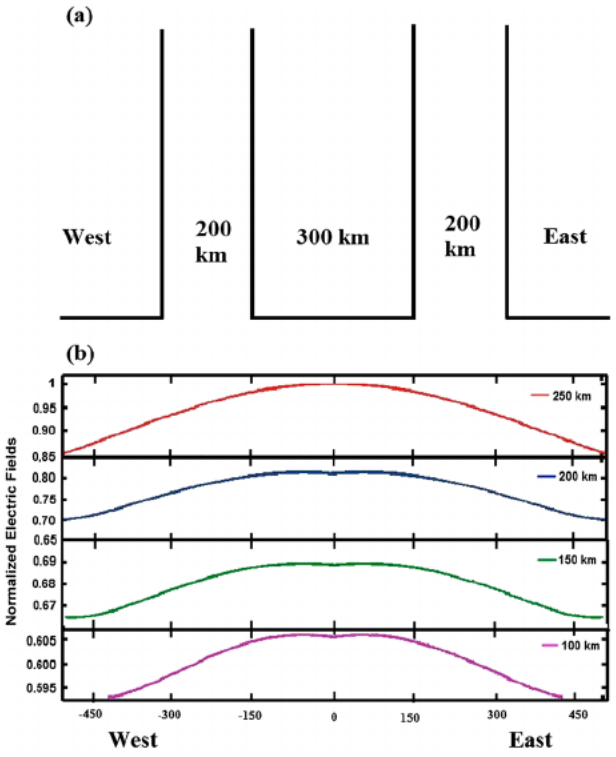

Figure 7. Same as Figure 6 but for capacitors with interplate separation $d = 200$ km. Direction of electric field is eastward.

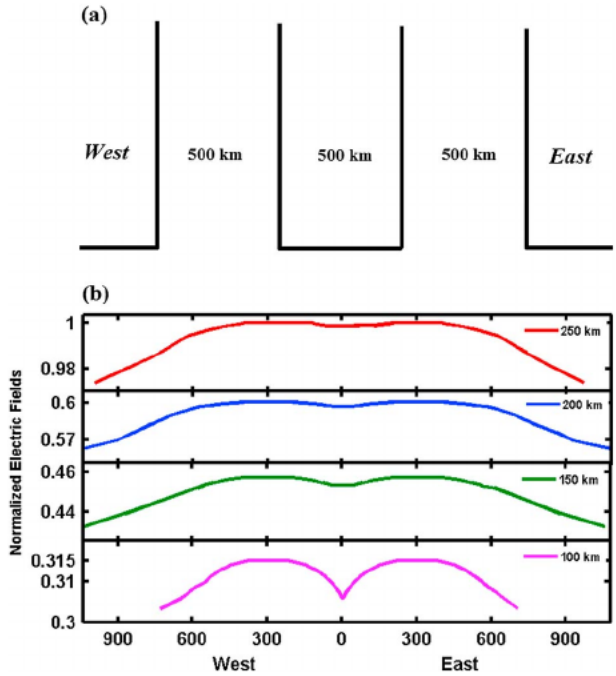

Figure 8. Same as Figure 6 but for capacitors with interplate separation of 500 km and intercapacitor separation of 500 km. Direction of electric field is eastward.

the bubble width, fringe field appears to be equivalent to that of a much wider bubble than a single bubble.

Figures 8a and 8b show results for the third case where both east-west bubble dimension and interbubble separation are 500 km. In this case, although fringe field extend to regions where overhead bubble is nonexistent, at lower altitudes, the east-west distribution of fringe field changes remarkably. Fringe field maximizes where the center of the bubble is located and decreases with increasing distance. These results are similar to those observed in the first case (Figure 6), implying that east-west distribution of fringe field depends on east-west bubble dimension and interbubble separation. In summary, we have shown that (1) fringe field decreases with decreasing altitude, (2) fringe field decreases significantly as we move away from the magnetic equator, (3) fringe field at a given height and latitude increases with increasing bubble width, and (4) in case of multiple bubbles, large fringe field is observed at the magnetic equator in regions where there exists no overhead bubble.

The finding that fringe field decreases with decreasing altitude is consistent with that noted earlier by *Alam Kherani et al.* [2004] and suggests that a highly depleted plasma bubble providing strong polarization charges would be required to produce necessary fringe field at the valley and *E* regions for the upward transportation of plasma and plasma irregularities. But a more important finding relevant for understanding the occurrence (nonoccurrence) of valley region irregularities at the equator (low latitudes) is the reduction of fringe field with latitude. It is also interesting to note that at low latitude, the fringe field just below the bubble decreases at a much faster rate than that at lower altitudes. Given the fact that plasma bubble develops vertically at the equator and maps to higher latitudes along field lines simultaneously, the polarization process in the low latitude close to the magnetic equator is believed to be quite similar, and the fringe fields both at the equator and

low latitudes on a local consideration would be same. But the fact that bubbles are magnetic field aligned and the fringe field at a low latitude point beneath the plasma bubble would be the vector sum of all field lines passing through it, the fringe fields are smaller than that at the equator. This reduction of fringe field is presumed to be one of the important reasons for impeding vertical transport of plasma and plasma irregularities at low latitudes.

We also found that the fringe field increases with increasing bubble width and in the case of multiple bubbles, fringe fields can be present even at locations where overhead bubble does not exist. This finding supports Jicamarca observations (shown in Figure 1) that valley region irregularities are observed in a region where there exists no overhead bubble [*Woodman and Chau*, 2001]. But no ascending type valley region irregularity has been observed in association with large-scale plume structures with bottomside undulation (Figure 2d) observed at Gadanki. Similar features were noted in earlier observations also [e.g., *Sekar et al.*, 2004]. There are however no concurrent measurements from magnetic equator and low latitude connected through common magnetic field lines to examine the contrasting aspect of valley region irregularities observed at the equator and low latitudes. Available observations however suggest that low-latitude valley region is not prone to instability during the growth phase of plasma bubble unlike that at the equator [*Yokoyama et al.*, 2005; *Patra and Rao*, 2007].

One aspect that needs some discussion is whether the fringe field is capable of generating irregularities in the valley region. The fringe field under consideration is eastward in the evening hours when plasma bubbles are in their growth phase. Eastward electric field (fringe field) could destabilize eastward electron density gradients in the valley region forming irregularities in the vertical direction, which could give rise to radar echoes. The fact that evening ionosphere often shows jagged electron density profile in the upper *E* region and valley region [e.g., *Prakash et al.*, 1972], gradient drift or interchange instability setting on vertical density gradients associated with jagged electron density profile could form zonal gradients in electron density. Upper *E* region irregularities displaying large-scale plasma wave structures have been observed in twilight hours (18:30–20:00 LT) at Jicamarca [*Chau and Hysell*, 2004]. These indicate that necessary background conditions, for forming plasma irregularities and more importantly large-scale zonal wave structures, can prevail in the equatorial upper *E* region. These irregularities however occur during twilight hours (prior to 20:00 LT) and do not show ascending pattern of the type reported by *Woodman and Chau* [2001] during the growth phase of plasma bubble (after 20:00 LT). However, if such horizontal structures are formed in the *E* region during the growth phase of plasma bubble, it is quite likely that they would be destabilized further and simultaneously transported upward by plasma bubble-associated fringe field. *Woodman* [1993] hypothesized that the ascending type valley region irregularities could be generated during the upward transport of the *E* region plasma by the plasma bubble-associated fringe field. These fringe fields could also destabilize upper *E* and valley region plasma through gradient drift instability if zonal electron density gradients exist. Moreover, for the growth of a large-scale plasma bubble at the *F* region, plasma has to be drawn from much lower altitude region [*Zalesak and Ossakow*, 1980], which is likely to alter the plasma density distribution in the region between the upper *E* and lower *F* regions. *Sekar et al.* [1997] demonstrated that indeed it takes place, and such an evolution of plasma density could give rise to plasma irregularities in the lower part of the *F* region (200–300 km), where the initial conditions are otherwise unfavorable for the generation of irregularities. *Basu* [1998] also verified the time-dependent property of the bottomside electron density distribution and provided quantitative description of such an effect. Required horizontal gradients could also be generated by strong longitudinal variation in upward plasma transport, and the fringe fields could destabilize the region of eastward electron density gradients. The fact that every plasma bubble event does not accompany ascending type valley region irregularities, it is quite possible that such a requirement is not fulfilled always. These processes account for much of the irregularities observed by the Jicamarca radar in association with plasma bubble (shown in Figure 1).

Given the fact that plasma depletion while growing in altitude extends latitudinally and large-scale electric field maps along magnetic field, we would expect somewhat similar to be observed at low latitude as well. Observations from low latitude such as Gadanki however are found to be different. In a recent study, *Aveiro and Hysell* [2012] have shown the inability of the equipotential field line approximation in reproducing three-dimensional structures of current in the bubble phenomenon. Their results showed large field-aligned current in association with the divergence of gravity-driven zonal current in the presence of plasma bubble. They also found that the same assumption leads to an underestimation of the growth rate of

plasma irregularities in their simulation study. In the present work, we find that fringe fields are smaller at low latitudes than at the magnetic equator, and this finding possibly indicates that magnetic field lines during plasma bubble phenomenon are not equipotential as shown by *Aveiro and Hysell* [2012]. Thus, it is quite likely that the reduced fringe field at low latitude as demonstrated in this work would possibly be insufficient to provide condition for generating irregularities in the valley region. Finite inclination of Earth's magnetic field at low latitudes could also be an important factor for reducing the growth of plasma instability unlike that at the magnetic equator where magnetic field lines are horizontal. An additional possibility for the contrasting equatorial and low-latitude observations may be spatially localized unstable plasma modes with maximum amplitude occurring at the magnetic equator [*Basu and Coppi*, 1983]. This mode was proposed by *Basu and Coppi* [1983] for the bottomside *F* region irregularities at the magnetic equator. Ascertaining this possibility for the upper *E* and valley regions however needs further investigation. Observations of valley region parameters, both plasma and neutral, at the equator and low latitude are necessary to understand the observed difference in the valley region irregularities.

5. Concluding Remarks

Results presented in this paper showed that observing valley region irregularities during the initial phase of equatorial plasma bubble at the magnetic equator and not observing at low latitudes could be linked with varying fringe field with latitude linked with the field-aligned nature of equatorial plasma bubble. Although it is not known whether fringe field can generate valley region irregularities, their presence and magnitude would be able to induce vertical transport of plasma or plasma irregularities, and their variation from the magnetic equator to low latitude at least partly is consistent with observations. Further work is necessary to understand their occurrence/nonoccurrence and their linkage to the equatorial plasma bubble parameters, viz., bubble dimension, depletion level, and height of occurrence.

Acknowledgments

Data used in this paper are available at NARL and are accessible through request. Figure 1 of this paper is a reproduction of Figure 1 of Woodman and Chau, GRL, 2001. The work was done at NARL when S. Mukherjee was visiting as a summer fellow of the Indian Academy of Sciences. S.M. gratefully acknowledges the Indian Academy of Sciences and NARL for supporting his research.

Alan Rodger thanks the reviewers for their assistance in evaluating this paper.

References

Alam Kherani, E., R. Sekar, and R. Raghavarao (2002), Equatorial rising structures in night-time E region: A manifestation of electrodynamical coupling of spread F, *J. Atmos. Sol. Terr. Phys.*, *64*, 1505–1510.

Alam Kherani, E., E. R. de Paula, and F. C. Bertoni (2004), Effects of the fringe field of Rayleigh-Taylor instability in the equatorial *E* and valley regions, *J. Geophys. Res.*, *109*, A12310, doi:10.1029/2003JA010364.

Alam Kherani, E., E. R. de Paula, R. Y. C. Cueva, and L. A. P. Camargo (2012), Observations of nighttime equatorial-upper-E-valley region irregular structures from Sao Luis radar and their occurrence statistics: A manifestation of vertical coupling between E and F regions, *J. Atmos. Sol. Terr. Phys.*, *75–76*, 64–70.

Aveiro, H. C., and D. L. Hysell (2012), Implications of the equipotential field line approximation for equatorial spread *F* analysis, *Geophys. Res. Lett.*, *39*, L11106, doi:10.1029/2012GL051971.

Basu, B. (1998), Equatorial plasma instability in time-dependent equilibrium, *Phys. Plasmas*, *5*, 2022–2028.

Basu, B., and B. Coppi (1983), Localized plasma depletion in the ionosphere and the equatorial spread F, *Geophys. Res. Lett.*, *10*, 900–903, doi:10.1029/GL010i009p00900.

Chau, J. L., and D. L. Hysell (2004), High altitude large-scale plasma waves in the equatorial electrojet at twilight, *Ann. Geophys.*, *22*, 4071–4076.

Choudhary, R. K., J.-P. St.-Maurice, L. M. Kagan, and K. K. Mahajan (2005), Quasi-periodic backscatters from the E region at Gadanki: Evidence for Kelvin-Helmholtz billows in the lower thermosphere?, *J. Geophys. Res.*, *110*, A08303, doi:10.1029/2004JA010987.

Hanson, W. B., and S. Sanatani (1971), Relationship between Fe^+ ions and equatorial spread *F*, *J. Geophys. Res.*, *76*, 7761–7768, doi:10.1029/JA076i031p07761.

Hanson, W. B., D. L. Sterling, and R. F. Woodman (1972), Source and identification of heavy ions in the equatorial *F* layer, *J. Geophys. Res.*, *77*, 5530–5541, doi:10.1029/JA077i028p05530.

Hysell, D. L., M. C. Kelley, W. E. Swartz, and R. F. Woodman (1990), Seeding and layering of equatorial spread *F* by gravity waves, *J. Geophys. Res.*, *95*, 17,253–17,260, doi:10.1029/JA095iA10p17253.

Parker, G. W. (2002), Electric field outside a parallel plate capacitor, *Am. J. Phys.*, *70*, 502, doi:10.1119/1.1463738.

Patra, A. K., and N. V. Rao (2006), Radar observations of daytime 150-km echoes from outside the equatorial electrojet belt over Gadanki, *Geophys. Res. Lett.*, *33*, L03104, doi:10.1029/2005GL024564.

Patra, A. K., and N. V. Rao (2007), Low-latitude valley region irregularities studied using the Gadanki radar, *J. Geophys. Res.*, *112*, A03303, doi:10.1029/2006JA011857.

Patra, A. K., P. B. Rao, V. K. Anandan, A. R. Jain, and G. Viswanathan (2002), Evidence of intermediate layer characteristics in the Gadanki radar observations of the upper E region field-aligned irregularities, *Geophys. Res. Lett.*, *29*(14), 1696, doi:10.1029/2001GL013773.

Prakash, S., B. H. Subbaraya, and S. P. Gupta (1972), Rocket measurements of ionization irregularities in the equatorial ionosphere at Thumba and identification of plasma irregularities, *Indian J. Radio Space Phys.*, *1*, 72–80.

Sekar, R., R. Sridharan, and R. Raghavarao (1997), Equatorial plasma bubble evolution and its role in the generation of irregularities in the lower *F* region, *J. Geophys. Res.*, *102*, 20,063–20,067, doi:10.1029/97JA01528.

Sekar, R., D. Chakrabarthy, R. Narayanan, S. Sripathi, A. K. Patra, and K. S. V. Subbarao (2004), Characterization of VHF radar observations associated with equatorial spread-F by narrow-band optical measurements, *Ann. Geophys.*, *22*, 3129–3136.

Venkateswara Rao, N., A. K. Patra, and S. V. B. Rao (2008), Some new aspects of low-latitude *E*-region QP echoes revealed by Gadanki radar: Are they due to Kelvin-Helmholtz instability or gravity waves?, *J. Geophys. Res.*, *113*, A03309, doi:10.1029/2007JA012574.

Woodman, R. F. (1993), Equatorial ionospheric irregularities as observed by the Jicamarca radar, in *Low-Lattitude Ionospheric Physics*, Proceedings of COSPAR Colloquium on Low Latitude, edited by F.-S. Kuo, pp. 83–95, Springer, New York.

Woodman, R. F., and J. L. Chau (2001), Equatorial quasiperiodic echoes from field-aligned irregularities observed over Jicamarca, *Geophys. Res. Lett.*, *28*, 207–209, doi:10.1029/2000GL000076.

Woodman, R. F., and C. LaHoz (1976), Radar observations of *F* region equatorial irregularities, *J. Geophys. Res.*, *81*, 5447–5466, doi:10.1029/JA081i031p05447.

Yamamoto, M., S. Fukao, R. F. Woodman, T. Ogawa, T. Tsuda, and S. Kato (1991), Midlatitude E region field-aligned irregularities observed with the MU radar, *J. Geophys. Res.*, *96*, 15,943–15,949.

Yokoyama, T., A. K. Patra, S. Fukao, and M. Yamamoto (2005), Ionospheric irregularities in the low-latitude valley region observed with the Equatorial Atmosphere Radar, *J. Geophys. Res.*, *110*, A10304, doi:10.1029/2005JA011208.

Zalesak, S. T., and S. L. Ossakow (1980), Nonlinear equatorial spread F: Spatially large bubbles resulting from large horizontal scale initial perturbations, *J. Geophys. Res.*, *85*, 2131–2142, doi:10.1029/JA085iA05p02131.